Research Square

Preprints are preliminary reports that have not undergone peer review.
They should not be considered conclusive, used to inform clinical practice,
or referenced by the media as validated information.

Study on hydroforming of 6061 Aluminum Alloy Sheet based on upper sheet

Xiao Jing Liu (lxj812@126.com)
Zhi He Zhang
Xue Feng
Chao Li
Ying Ying Zhou

Research Article

Keywords: double-layer sheet hydroforming, numerical simulation, BP neural network, constitutive model, pre-bulging

Posted Date: March 18th, 2022

DOI: https://doi.org/10.21203/rs.3.rs-1449154/v1

License: This work is licensed under a Creative Commons Attribution 4.0 International License.
Read Full License

Study on hydroforming of 6061 Aluminum Alloy Sheet based on upper sheet

Xiao Jing Liu* • Zhi He Zhang • Xue Feng Ma • Chao Li • Ying Ying Zhou

Abstract: Forming large-size thin-walled hemispherical parts by hydroforming is often accompanied by serious wall thickness thinning，instability and rupture of the suspending area. In order to solve the appeal problems, this paper adopts the combination of finite element numerical simulation analysis and experimental verification, and takes the 6061-T6 aluminum alloy thin-walled hemispherical part as the research object to carry out the formability analysis of double-layer sheet hydroforming. In order to improve the accuracy of numerical simulation, uniaxial tensile tests of AA6061-T6 tensile specimens were carried out, and a BP neural network prediction model that can truly reflect the plastic deformation characteristics of materials was established. In this paper, the wall thickness and the contact status between punch and sheet are used as the evaluation indexes to simulate and analyze the hydroforming of the double-layer sheets, and the process flow of the single-sheet and the double-layer sheet hydroforming was compared and analyzed. The forming law of sheet metal under different friction coefficient between sheets and different upper sheet thickness was explored. Finally, the optimal process conditions were used for forming experiments, and the results were basically consistent with the simulation results.

Keywords: double-layer sheet hydroforming, numerical simulation, BP neural network, constitutive model, pre-bulging

1. introduction

6061 - T6 aluminum alloy is an Al-Mg-Si alloy with high hardness, high specific strength, good corrosion resistance and uniformity. It is the best choice for materials with low price and high quality, and is widely used in aerospace, automobile, weapons and other fields [1–2]. However, in the production process, some thin-walled parts with large curvature are prone to instability and fracture, wrinkle and other defects in the ordinary hydroforming technology. At this time, it is necessary to introduce the double-layer sheet hydroforming technology to improve it. Due to the high cost of materials and long production cycle of double-layer sheet hydroforming, it is necessary to simulate the forming process of precision parts by finite element software. The accurate establishment of material constitutive model is the most critical step in numerical simulation. In order to construct the constitutive model of 6061-T6 aluminum alloy with high precision, this paper conducts uniaxial tensile test on AA6061-T6 tensile samples. The back propagation (BP) neural network model was used to construct the constitutive model of 6061 - T6 aluminum alloy [3].

Xiao Jing Liu(*)·Zhi He Zhang·Xue Feng Ma·Chao Li·Ying Ying Zhou
School of Materials Science and Engineering,
Harbin University of Science and Technology,
150040 Harbin, China
e-mail: zhangzhihe323@163.com

Traditionally, the double-layer sheets as a composite sheet that combines the two-layer metal sheets through cold rolling, hot rolling and pressure welding [4]. In recent years, scholars in China and abroad have referred to the excellent performance of multi-layer composite sheets and mechanically superimposed two-layer metal sheets, which are generally upper sheets with good formability and formed sheets with poor formability. In this way, the forming quality of formed sheets can be improved [5].

The double-layer sheet hydroforming technology was formally proposed by Hao Dong [6] from Harbin Institute of Technology to form the elliptical bottom of rocket propellant. By comparing the two different forming methods of single-layer sheet and double-layer sheet, the positive effect of double-layer sheet hydroforming technology on sheet forming was proved. In 2016, Jiu Hong Zhou [7] conducted a research on the double-layer sheet hydroforming technology for tailor-welded sheets. Through the upper sheet research with different thicknesses,

different materials and different surface states, the optimal upper sheet parameters for forming the bottom of the tank of the rocket launcher were explored. In the same year, the scholars of Harbin Institute of Technology discussed the influence of upper sheet on the bulging of aluminum alloy sheet and tailor-welded sheets respectively [8,9], and proved the positive effect of upper sheet on forming sheet theoretically and experimentally. Subsequently, Tie Jun Gao [10] analyzed the upper layer of different materials by bulging experiments. The results show that the better the plasticity, the higher the strength and hardening index of the upper layer, the more conducive to the forming performance of the formed plate. Bin Jun Zhou et al. [11-13] used numerical simulation and experiment to explore the mechanism of defect suppression in double-layer sheet hydroforming, and made clear the principle of selecting upper layer.

In addition, Alireza [14], explored the factors affecting the fracture of the parts in the double-layer sheet hydroforming, and explored the critical fracture pressure of the conical parts. Molaei [15] studied the hydroforming of conical parts with double-layer sheets. The results showed that the higher the strength and formability of the upper layer, the greater the drawing ratio of the parts.

Due to the large-size thin-walled hemispherical parts, there are some defects such as wrinkling and thinning in the suspending area of the parts in the traditional drawing forming. This paper will take the hemispherical surface parts as the research object, and further explore the forming mechanism and the optimization scheme of the forming process of the double-layer sheet hydroforming parts under the condition of establishing the upper sheet material, so as to provide reference for the study of the problems such as easy wrinkling and thinning in the suspending area of the surface parts in the forming process.

2. Process principle and theoretical analysis

2.1 principle analysis of double-layer sheet

The forming principle of the double-layer sheet hydroforming technology is shown in Figure 1. This technology is mainly aimed at the problem that the thinner curved sheet parts are easy to wrinkle in the drawing process. By placing a layer of thicker metal sheet on the metal sheet to be formed, the thickness of the plate that needs to be formed is artificially increased, and the problem that the ultra-thin plate is easy to wrinkle in the drawing process is reduced. At the same time, the forming limit is further improved by using the beneficial interfacial friction between the two sheets. Reasonable process parameters are adopted in the drawing process. After forming, the springback of the two-layer metal sheet is different, so that the two-layer sheet is naturally separated to obtain the target part.

(a) Deep drawing process (b) Two-layer sheet separation (c) Target part

Fig. 1 Schematic of double-layer sheet hydroforming

The mechanical properties of the upper sheet should meet the following conditions in the double-layer sheet hydroforming：

1. The yield strength of the upper sheet should be less than the formed sheet. During the forming process, the upper sheet will yield earlier than the formed sheet, thus leading to plastic deformation of the formed sheet;

2. The tensile strength of the upper sheet should be greater than formed plate. Under the action of excessive drawing force and hydraulic pressure, the fracture trend of the upper sheet is less than formed sheet, which avoids the poor forming quality of the parts caused by the fracture of the upper sheet;

3. There is a large difference in the elastic modulus between the double-layer sheets. After

forming, the two-layer sheets are separated due to different springback values, so that the target parts can be easily obtained.

In this paper, 1Cr18Ni9Ti stainless steel selected as the upper sheet material. The mechanical properties of the formed sheet and the upper sheet are compared as follows, which meets the selection conditions of the above three upper sheets.

Tab.1 Mechanical property of the sheet of AA6061-T6 and 1Cr18Ni9Ti

	Yield strength σ_s /MPa	Tensile strength σ_b / MPa	Elastic modulus/ GPa	Poisson ratio	Elongation /%
AA6061-T6	276	310	68.9	0.33	12
1Cr18Ni9Ti	200	550	118.6	0.33	40

2.2 Theoretical Calculation of Critical hydraulic pressure

The Critical hydraulic pressure is the minimum chamber pressure required for the sheet in the flange area to lift slightly under the chamber pressure. At this time, the liquid in the chamber can overflow between the sheet and the die, which can produce fluid lubrication between the die and the sheet. The critical hydraulic pressure is an important parameter in the hydroforming process, and it is the key to improve the forming limit of the material.

At the corner of the die, the force required for the sheet to be lifted is equal to the force of the liquid chamber pressure acts on the sheet. The material with the width of Δy at the corner of the die is analyzed and can be approximated as a small rectangle, so the formula for calculating the critical hydraulic pressure can be obtained as follows：

$$\sigma_w \cdot \Delta y \cdot t = P_{cr}(R_d + d - t) \text{——(1)}$$

In the formula, σ_w is the tensile stress of the sheet at the corner of the die, t is the thickness of the sheet, P_{cr} is the critical hydraulic pressure, R_d is the radius of the spherical die corner, d is the distance between the sheet and the die.

Because the tensile stress of the sheet at the corner of the die is：

$$\sigma_w = \frac{\sigma_b t}{2R_d + t} \text{——(2)}$$

where σ_b is the tensile strength of the material, and it can be obtained from Formulas (1) and (2) :

$$P_{\text{cr}} = \frac{\sigma_b t^2}{(2R_d + t)\cdot(R_d + d - t)} \text{——(3)}$$

The tensile strength of 6061 - T6 is 310 MPa, and the corresponding critical hydraulic pressure is 1.47 MPa. Therefore, in the subsequent exploration of the best hydraulic pressure curve, the minimum value of the whole curve should be greater than 1.47 MPa.

3. The establish of neural network

3.1 Tensile specimen and scheme

Tab.2 Chemical composition of 6061-T6 aluminum alloy

element	Si	Mg	Fe	Cu	Mn	Cr	Zn	Ti	Al
content /wt%	0.6	1.0	0.7	0.28	0.15	0.20	0.25	0.15	Margin

In order to construct the constitutive model of 6061 - T6 aluminum alloy, 2 mm tensile specimens were selected in this paper. According to the ISO 204:1997 standard, the specimens were prepared by wire cutting. The tensile specimens are shown in Figure 2(a,b).

(a) (b) (c)

Fig. 2 The tensile specimen and MTS universal electronic testing machine

The tensile test was carried out at three strain rates and six temperatures. The specific test scheme is shown in table 3. Each test was repeated three times and the median was taken to reduce the test error. The tensile equipment is MTS universal electronic testing machine. The accuracy level of the equipment is 05, and the maximum tensile force can reach 20 KN. At the same time, the equipment has a heating furnace. The equipment is shown in Figure 2(c). In order to ensure the temperature uniformity in the furnace during thermal tensile, the temperature of the heating furnace was set as the target temperature and maintained for 30 min. The holding sample was put into the heating furnace, and the tensile test was started after holding for 10 min.

Tab.3 6061-T6 aluminum alloy hot tensile test program

Test number	Strain rate /s^{-1}	Temperature /℃	Test number	Strain rate /s^{-1}	Temperature /℃
1	10^{-1}	25	10	10^{-1}	150
2	10^{-2}	25	11	10^{-2}	150
3	10^{-3}	25	12	10^{-3}	150
4	10^{-1}	50	13	10^{-1}	200
5	10^{-2}	50	14	10^{-2}	200
6	10^{-3}	50	15	10^{-3}	200
7	10^{-1}	100	16	10^{-1}	250
8	10^{-2}	100	17	10^{-2}	250
9	10^{-3}	100	18	10^{-3}	250

3. 2 Test result analysis

The tensile results of 6061 - T6 specimens at different strain rates at 25 °C are shown in Figure 3. The tests were carried out at 10^{-1}、10^{-2}、10^{-3} strain rates, respectively.

Fig.3 Tensile test results at different strain rates at 25 °C

In order to construct the constitutive equation of 6061-T6 aluminum alloy, the uniaxial tensile test data need to be processed. And draw the real stress-strain curve, get the real stress-strain curve as shown in Figure 4.

By observing the stress-strain curve under the same strain rate in Figure 4, it can be found that with the increase of temperature, the yield strength of the material gradually decreases, the elongation gradually increases, and the forming performance of the material has been effectively improved. This is because the increase in temperature increases the part of the internal structure of the material involved in dynamic recovery and dynamic recrystallization,

which can offset certain work hardening; on the other hand, the critical shear stress between atoms decreases, the slip system and slip mode increase, and plastic deformation is more likely to occur. In addition, the increase of temperature makes the second-phase particles in the aluminum alloy material easier to integrate into the matrix, thus weakening the influence of the second-phase strengthening, and improving the elongation and plastic deformation ability of the material. By observing the stress-strain curves at the same temperature, it can be seen that the smaller the strain rate is, the smaller the elongation and yield strength of the material are. This is because the recovery and recrystallization time of the material decreases with the increase of strain rate, and the effect of offsetting work hardening is more limited, so the yield strength increases gradually.

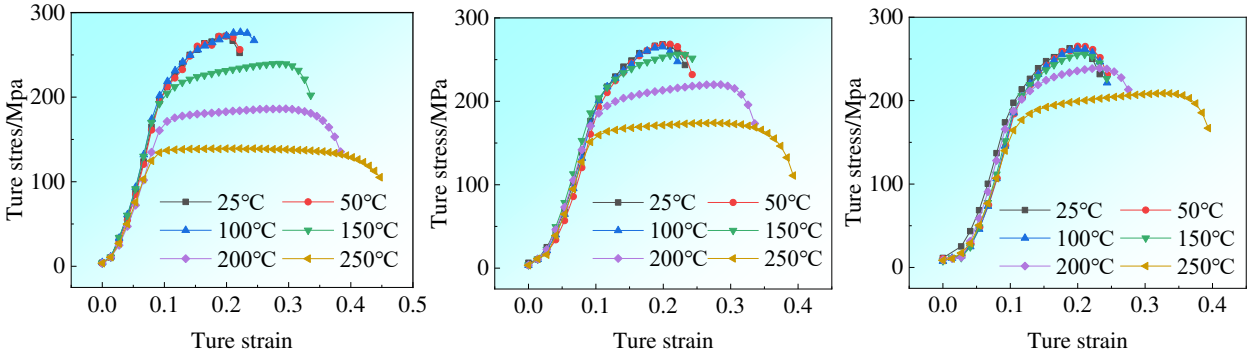

(a) $\dot{\varepsilon}$=0.001 (b) $\dot{\varepsilon}$=0.01 (c) $\dot{\varepsilon}$=0.1

Fig. 4 The true stress-strain curve at different strain rates

4. Construction of material constitutive model

4. 1 The establishment of BP neural network model

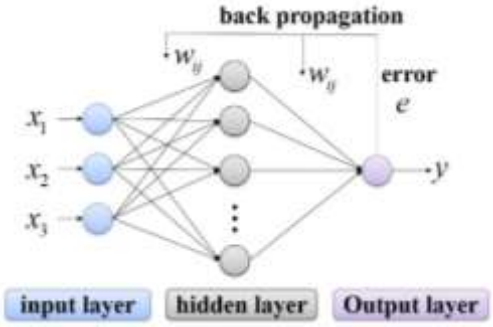

Fig. 5 Neural network structure

The BP neural network model consists of three parts, namely, the input layer, the hidden layer and the output layer. The network structure is shown in Figure 5. The input signal is transmitted from the input point to the hidden point, and finally to the output point through the adjustment of the weight between layers. Through the comparison of errors, the weight is corrected, and then the back propagation is carried out until the target error is reached. In addition, the input value of each node is the sum of the weights of the output values of all nodes in the previous layer, and the output value of each point is determined by the node input, the activation function and the bias. Therefore, the network can achieve a highly nonlinear mapping from input to output.

The number of hidden layer neurons will affect the accuracy of BP neural network, too much will lead to over fitting. On the contrary, too little will lead to low accuracy of simulation training. In this paper, due to the small amount of data, the single hidden layer structure is selected. The number of neurons in the hidden layer is obtained according to the empirical formula. The formula is:

$$\delta = \frac{N}{a(m+n)} \quad \text{——(4)}$$

where δ is the number of neurons, N is the number of training samples, n is the number of neurons in the output layer, m is the number of neurons in the output layer, and a is the adjustment parameter.

In this paper, temperature, strain, strain rate as the input layer, stress as the output layer, namely m = 3, n = 1. The number of training samples is 360. After repeated experiments, it is determined that when a = 3, that is, when the number of hidden neurons is 30, the performance of the network structure is the best.

The transfer function of hidden layer is Sigmoid function, and its form is：

$$f(x)=\frac{1}{1+e^{-x}} \quad \text{——(5)}$$

The input form is：

$$net=x_1\omega_1+x_2\omega_2+x_3\omega_3+\cdots+x_n\omega_n \quad \text{——(6)}$$

The output form is：

$$y=f(\ net\ )=\frac{1}{1+e^{-net}} \quad \text{——(7)}$$

The training function uses Trainlm function to improve the BP algorithm. The improved BP neural network has smaller mean square error, high precision and fast convergence speed.

4.2 Data processing

Data normalization can convert all the experimental data into the value of 0-1 interval, which can effectively avoid the influence of experimental data floating on the accuracy of neural network. The formula is as follows :

$$Y=0.1+0.8\times\frac{ax-\min a}{\max a-\min a} \quad \text{——(8)}$$

In the formula: Y is the normalized data, $min\,a$ is the minimum value in$a$class, $max\,a$is the maximum value in a class. Due to the large difference between the strain rate values, the use of the above formula will lead to a large difference between the real value and thus affect the accuracy of training, so the following formula is used to deal with the strain rate.

$$\dot{\varepsilon}=\frac{(3+\lg\dot{\varepsilon}-0.95(3+\lg\dot{\varepsilon}_{min}))}{1.05(3+\lg\dot{\varepsilon}_{max})-0.95(3+\lg\dot{\varepsilon}_{min})} \quad \text{——(9)}$$

424 data were selected from the real stress-strain curve, including 360 training samples and 64 data for verification. After simulation, the target accuracy is set to 0.001, the learning rate is 0.001, and the maximum number of learning times is 1100.

4.3 Result analysis

In order to explore the relationship between the output stress value and the actual stress value, the output stress value needs to be processed, as follows:

$$\sigma=\sigma_{min}+1.25(\sigma_n-0.1)(\sigma_{max}-\sigma_{min}) \quad \text{——(10)}$$

where$\sigma$is the predicted true stress value, σ_n is the normalized stress value, σ_n is the minimum value in the stress test sample, and σ_{max} is the maximum value in the stress test sample.

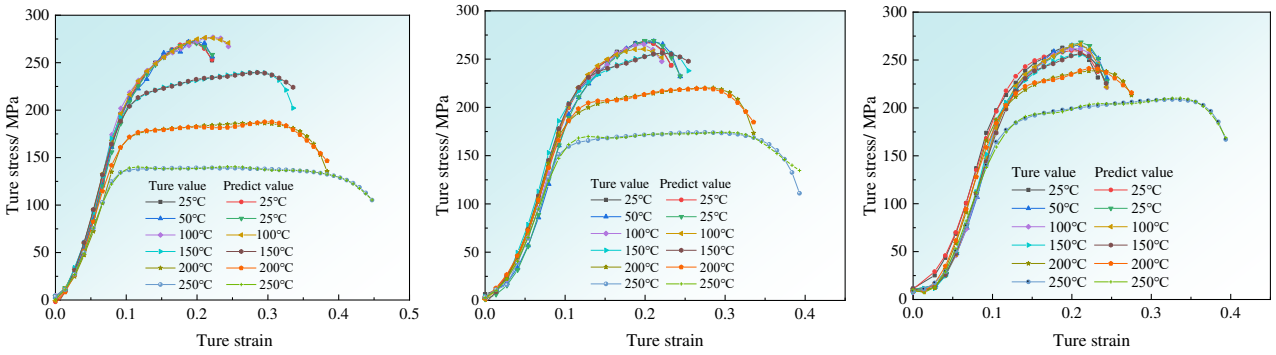

(a) When the strain rate is 0.001 (b) When the strain rate is 0.01 (c) When the strain rate is 0.1

Fig. 6 Comparison between predicted and experimental values of BP neural network

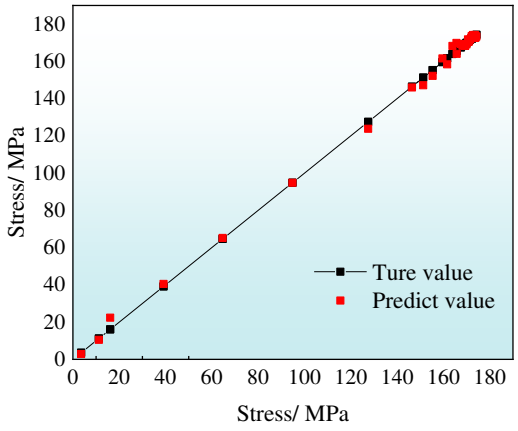

Fig. 7 Correlation curve

Figure 6 is the comparison between the predicted stress value and the experimental value of BP neural network. Figure 7 is the fitting curve, and the fitting coefficient is 0.9989, which has a high correlation. Table 4 shows the comparison of some predicted values and experimental values when the strain rate is 0.01. According to the error situation, it can be seen that the overall error is within 5 %, the minimum error

is 0.05 %, and the average error is 0.92 %. The constitutive model constructed by neural network has high accuracy. The application of this constitutive model has practical guiding significance for subsequent numerical simulation

Tab. 4 Comparison of predicted and experimental values at strain rate of 0.01

Temperature /°C	Strain	experiment / MPa	predict/ MPa	relative error /%	Temperature /°C	Strain	experiment/ MPa	predict/ MPa	relative error /%
25	0.05	70.24	70.20	0.06	150	0.05	78.54	74.87	4.67
25	0.10	201.28	199.56	0.85	150	0.10	203.85	203.53	0.16
25	0.15	248.91	249.34	0.17	150	0.15	239.14	240.45	0.55
25	0.20	268.32	267.49	0.31	150	0.20	252.91	252.55	0.14
50	0.05	56.91	56.08	1.46	200	0.05	73.11	72.37	10.1
50	0.10	192.90	189.42	1.80	200	0.10	185.60	186.33	0.39
50	0.15	245.94	245.19	0.30	200	0.15	206.18	207.03	0.41
50	0.20	267.61	269.03	0.53	200	0.20	213.20	213.31	0.05
100	0.05	64.67	66.37	2.63	250	0.05	64.64	65.15	0.79
100	0.10	200.99	200.66	0.16	250	0.10	159.58	161.56	1.24
100	0.15	244.17	249.63	2.24	250	0.15	168.23	168.38	0.09
100	0.20	265.40	260.32	1.91	250	0.20	171.44	171.63	0.11

5. Numerical simulation scheme design

5.1 Establishment of finite element model

This paper takes the hemispherical parts as the research object, and the specific part size is shown in Figure 8. According to the part size, choose 170mm round billet.

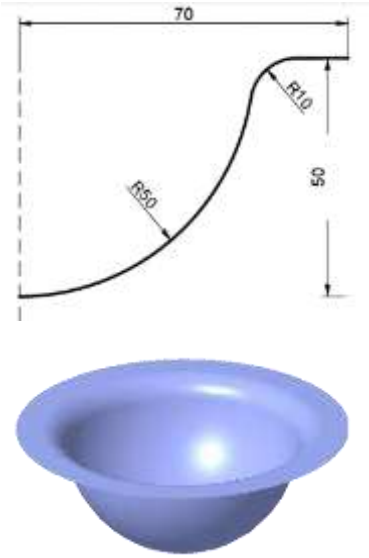

Fig. 8 Size and shape of parts

In this paper, ABAQUES software was selected for the numerical simulation of the double-layer sheet hydroforming. The fixed gap method was used in the modeling, that is, the gap between the blank holder and the die flange is 1.1 times the sheet thickness. In the software, the global friction was set by tangential ' penalty ' friction, and the global friction coefficient is 0.15. Due to the fluid lubrication effect, the friction between the die and the sheet is 0.04. At the same time, because the hemispherical parts are axisymmetric parts, in order to reduce the time of software operation, only half of the finite element model was analyzed. The mesh was divided by the central axis algorithm, and the minimum mesh was filtered. The unit shape was quadrilateral. The finite element model of hemispherical parts is shown in Figure 9.

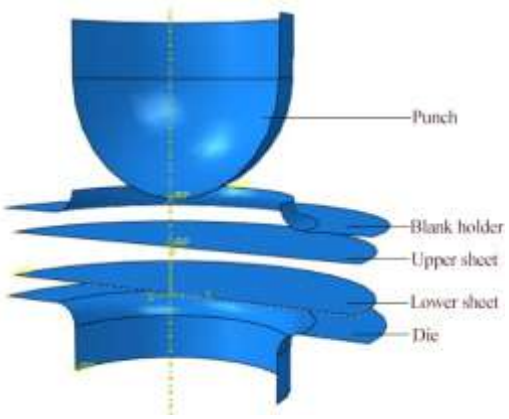

Fig. 9 The finite element model of double-layer sheet hydroforming

5.2 Process analysis

5.2.1 Influence of hydraulic pressure on Part forming

The 1Cr18Ni9Ti stainless steel upper sheet with 1.5 mm thickness was selected to simulate the double-layer sheet hydroforming. The time step of the whole forming process was set to 1 s, where 0 ~ 0.8 s is the drawing stage and 0.8 ~ 1 s is the pressure maintenance stage. In ABAQUS software, the pressure was applied to the lower surface of the sheet to simulate the hydraulic pressure in actual production. When the initial hydraulic pressure was 2 MPa and the time step was 0.8 s, the hydraulic pressure increased to 10 MPa, 15 MPa, 20 MPa, 25 MPa and 30 MPa, respectively. The hydraulic loading path diagram is shown in Figure 10.

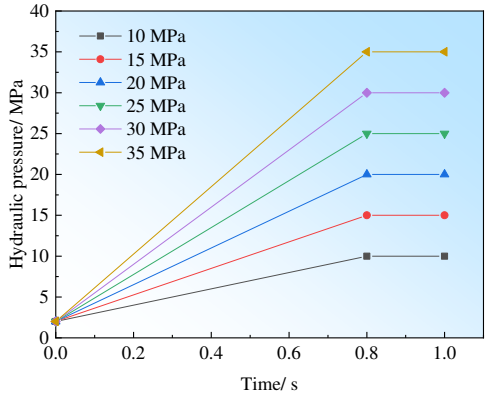

Fig. 10 Hydraulic pressure loading path

On the formed parts, the node path from the center point to the edge node was selected along the radius direction, as shown in Figure 11. The coordinates of each element node are used to represent the contour shape of the parts. The contour comparison diagram of the parts under different pressure loading paths is shown in Figure 12. It can be found that the greater the hydraulic pressure is, the better the fittability of the parts is.

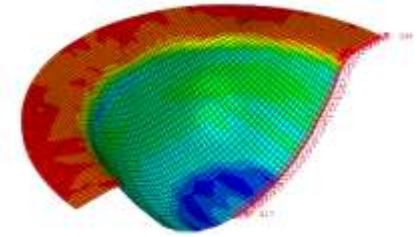

Fig. 11 path of node

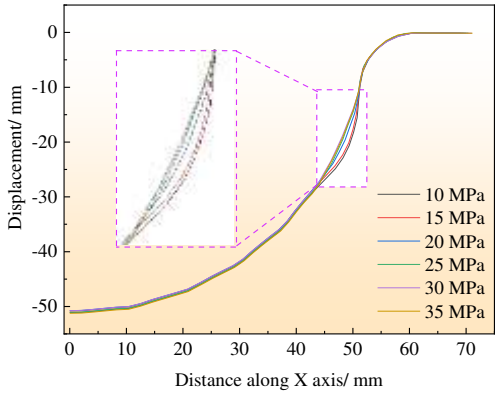

Fig.12 The comparison of part contour under different hydraulic loading paths

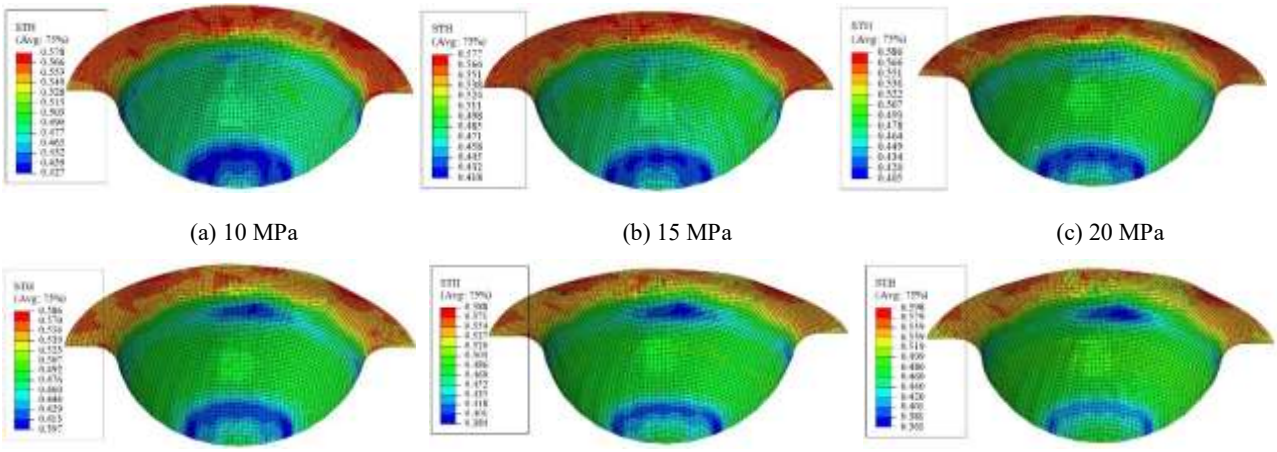

(a) 10 MPa (b) 15 MPa (c) 20 MPa

(d) 25 MPa (e) 30 MPa (f) 35 MPa

Fig. 13 The part wall thickness distribution under different hydraulic loading paths

By observing the wall thickness distribution of Figure 13, it can be found that with the increase of the hydraulic pressure, the defect of wrinkling in the suspending area has been significantly improved, but also accompanied by the thinning of the wall thickness of the suspending area. When the hydraulic pressure was 20 MPa, there was slight wrinkle in the part suspending area. The minimum wall thickness of

the suspending area was 0.434 mm, and the thinning rate was 13.2 %. At 35 MPa, the maximum thinning rate of the suspending area reached 27. 8 %, and the actual forming fracture risk is large.

With the increase of hydraulic pressure, the thinning range of punch contact area decreases, but at the same time, the thinning of wall thickness was accompanied. At 10 MPa, the minimum wall thickness of the region was 0.427 mm, and the wall thickness of the center of the ball bottom was 0.490 mm, with a difference of 0.063 mm. With the increase of hydraulic pressure, the difference between the minimum wall thickness of the punch contact area and the center wall thickness of the ball bottom gradually increases. At 35 MPa, the minimum wall thickness of the punch contact area was 0.381 mm, and the wall thickness of the center of the ball bottom was 0.460 mm, with a difference of 0.079 mm.

When the pressure was 20 MPa, the wall thickness thinning rate of the suspending area of the part was small, and the fittability of the parts was improved. At the same time, the wall thickness distribution of the part was relatively uniform, so 20 MPa was selected as the optimal hydraulic pressure for the forming of the part.

5.2.2 Effect of pre-bulging on forming performance of parts

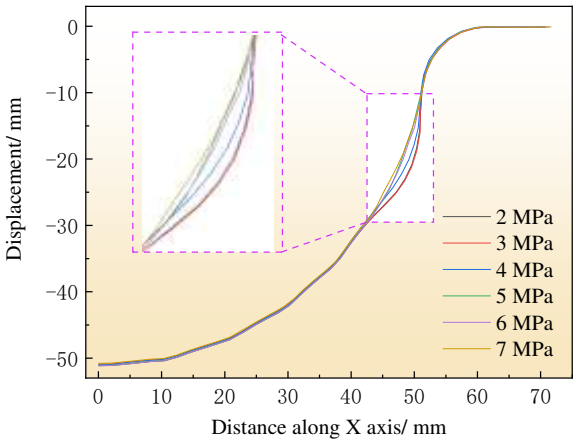

Fig. 14 The comparison of part contour under different pre-bulging pressures

Since there is still wrinkling in the suspending area when the hydraulic pressure was 20 MPa, the pre-bulging process is introduced to improve it. The pre-bulging is the process of sheet metal forming close to the punch by reverse bulging under the action of hydraulic pressure before the punch downward. Set 0 ~ 0.1 s to pre-bulging stage; 0.1 ~ 0.8 s was the drawing stage; 0.8 – 1 s was the pressure maintenance stage. Considering the pre-bulging of hemispherical base, the fixed pre-bulging height should be 0 mm. The pre-bulging pressures of 2 MPa, 3 MPa, 4 MPa, 5 MPa, 6 MPa and 7 MPa were selected for simulation. The contour diagram of the parts is shown in Figure 14.

Through Figure 14, it can be found that the larger the pre-bulging pressure is, the better the fittability of the parts is, and the wrinkle in the suspending area is effectively suppressed. However, by observing Figure 15, it can be found that the wall thickness of the core area of the sheet increases with the increase of the pre-bulging pressure, and the wall thickness of the annular region at the bottom of the sheet decreases with the increase of pre-bulging pressure.

This phenomenon can be summarized as follows: When the pre-bulging pressure is small, the inverse bulging height of the sheet metal is small, that is, the area of the sheet metal contact to the punch is small, resulting in an increase in the area of the suspending area and increasing the risk of sheet instability and wrinkling. Therefore, obvious wrinkling occurs in the suspending area. When the pre-bulging pressure is large, the inverse bulging and thinning of the sheet metal is serious, and the friction resistance of the punch to the flow of the central sheet metal to the surrounding is also increased. Therefore, the part has a serious thinning in the ring area. According to the thinning and wrinkling of the wall thickness, the optimal pre-bulging pressure was finally selected as 4 MPa.

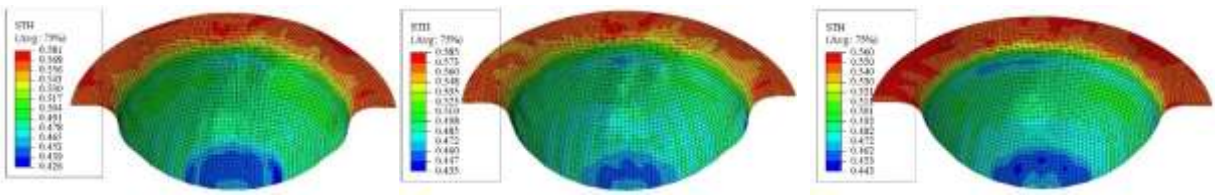

(a) 2 MPa (b) 3 MPa (c) 4 MPa

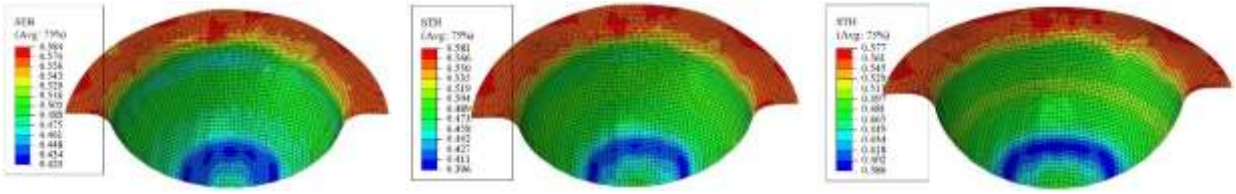

(d) 5 MPa (e) 6 MPa (f) 7 MPa

Fig. 15 The parts wall thickness distribution under different pre-bulging pressures

5.3 Numerical simulation analysis of single sheet and double-layer sheet hydroforming

Fig. 16 shows the wall thickness distribution with good quality formed by single sheet and double-layer sheet hydroforming. it can be seen that the minimum wall thickness of the single-layer sheet part is 0.37 mm, and the maximum thinning rate is 26 %. At this time, the part has broken, and the sheet thickness at the corner of the die has also increased by 10 %, and there is a wrinkle trend. The minimum wall thickness of the double-layer sheets forming part is 0.443 mm, and the maximum thinning rate is 11.4 %. According to the wall thickness comparison curve in Figure 17, it can be found that during double-layer sheet hydroforming, the upper sheet has obvious improvement effect on the wall thickness of the part suspending area, and the wall thickness distribution is also more uniform, avoiding the wrinkling of the suspended area. At the same time, the area of wall thickness thinning in the punch contact area was also smaller. The introduction of upper sheet makes this thin-walled part have good formability.

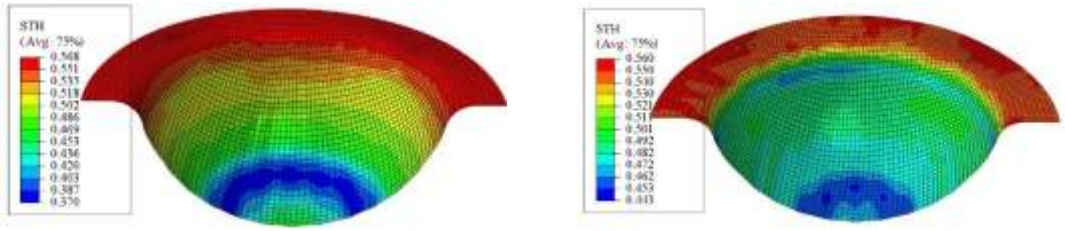

(a) (b)

Fig. 16 Forming wall thickness distribution

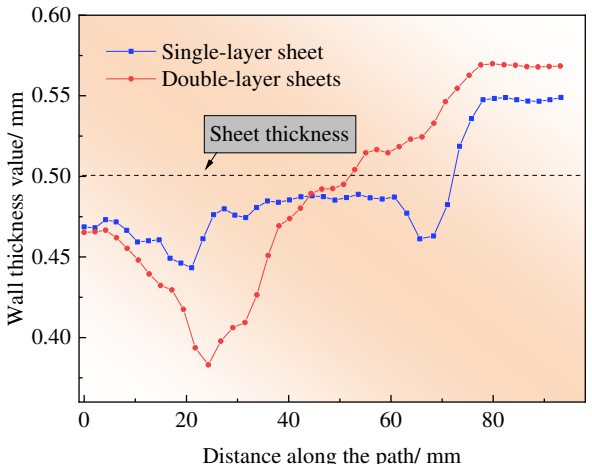

Fig. 17 Wall thickness comparison

In order to explore the influence of different inter-sheet coefficients on the forming quality of the formed plate, the friction coefficients of 0.05, 0.1, 0.15, 0.2, 4 groups were simulated and analyzed on the basis of the above process parameters. Figure 18 is the contour diagram under different friction coefficients. It can be found that the change of friction coefficient has little effect on the contour shape of parts. The wall thickness contours of the parts under different friction coefficients are shown in Figure 19.

5.4 Effect of upper sheet conditions on formability of parts

5.4.1 Friction coefficient between sheets

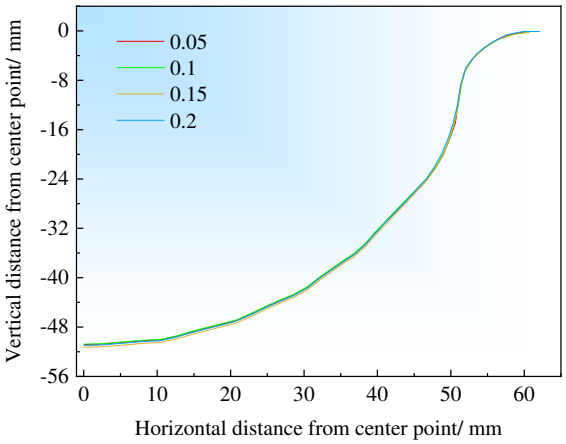

Fig. 18 Part contour maps under different friction coefficients

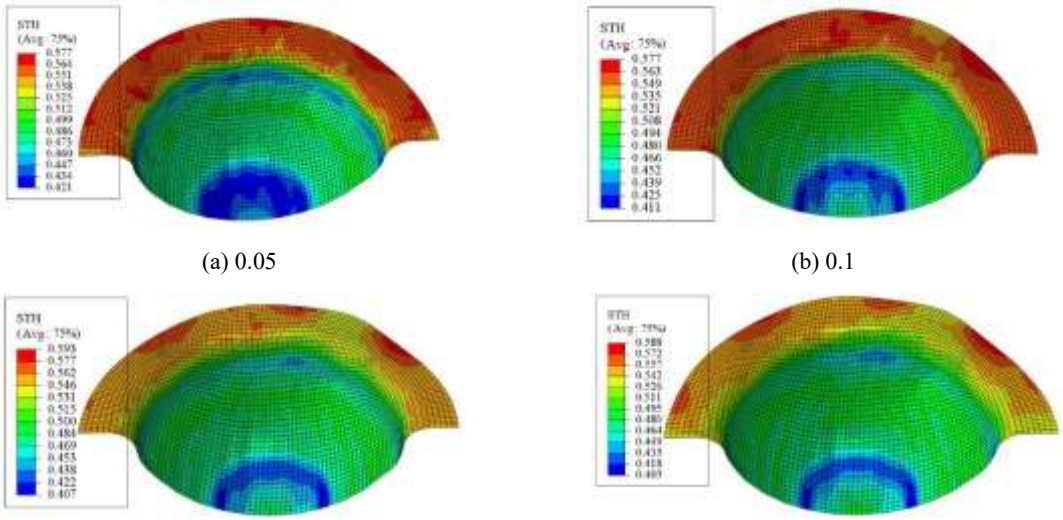

(a) 0.05 (b) 0.1

(c) 0.15 (d) 0.2

Fig. 19 Parts Wall thickness distribution under different friction coefficients

By observation, the parts thinning occurs at the ball bottom and suspending area. With the increase of friction coefficient, the thickness thinning area of the ball bottom gradually decreases, and the thickness thinning is accompanied. When the bulging begins, the upper sheet and the forming plate occur inverse bulging thinning together. When the friction coefficient was 0.05, the radial friction force of the upper sheet on the formed plate was small, and the flow ability of the sheet in the non-bulging area to the bulging area was strong, so the wall thickness distribution of the ball bottom plate is relatively uniform. With the increase of the friction coefficient, the flow resistance of the upper sheet on the formed sheet increases, resulting in the thinning of the ball bottom ring. At the same time, the flow of the sheet at the center of the ball bottom is relatively difficult, and the wall thickness reduction is small.

The thinning of the sheet suspending area is mainly caused by the failure of the sheet in the flange area to flow into the suspending area in time. When the friction coefficient was 0.05, the most dangerous area in the suspending area was 0.447 mm, and the thinning rate was 10.6 %. When the friction coefficient was 0.1, the wall thickness at the ring of the suspending area was 0.466 mm, and the thinning rate was 6.8 %. With the increase of the friction coefficient, this area continues to thinning, and the flange edge area also shows a small range of thickening. When 0.15 – 0.2, the maximum wall thickness was about 0.590 mm, and the thickening rate was 18 %. Due to the increase of inter-sheet friction and the increase of wall thickness in flange area, it is difficult to supplement materials in the suspending area and gradually reduce the thickness. Considering the friction coefficient in the punch contact area should not be too small, otherwise，the coordinated deformation effect between the two plates will be weakened. By comparison, the most obvious friction coefficient for wall thickness improvement is

0.1.

5.4.2 Thickness of upper layer

In order to explore the influence of the upper sheet thickness on the formed sheet, under the same hydraulic pressure conditions, the upper sheet of 1 mm, 1.5 mm and 2 mm thickness were selected to assist the forming of 0.5 mm sheet. The loading path of the hydraulic pressure is shown in Figure 20.

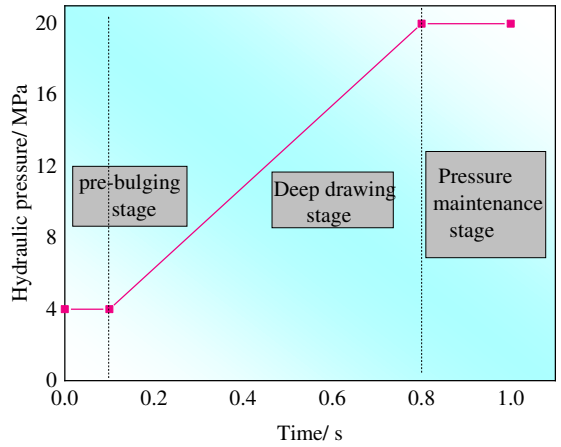

Fig. 20 Hydraulic pressure loading path

Figure 21 shows the contour diagram of the parts under different upper sheet thicknesses. It can be seen

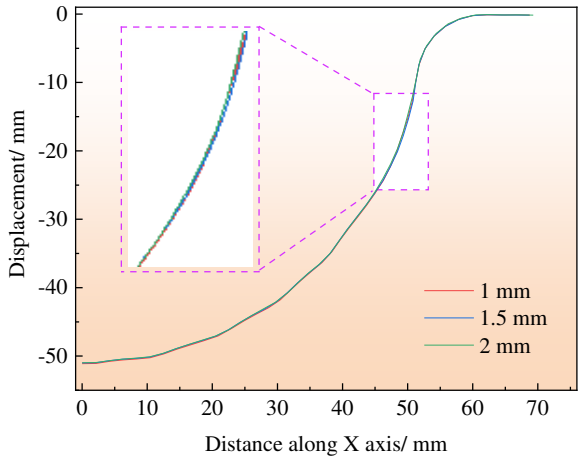

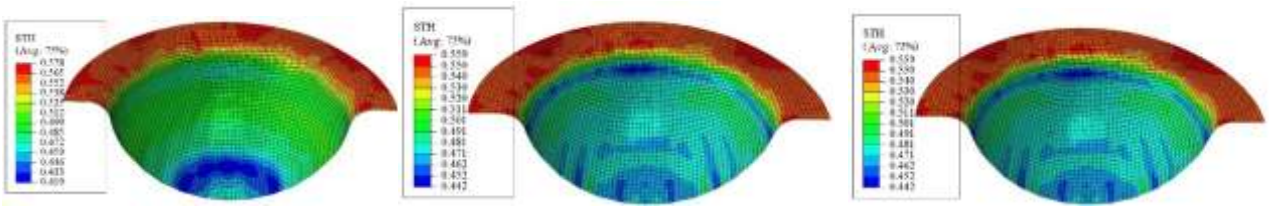

Fig.21 The comparison of parts contour under different upper sheet thicknesses

that the upper sheet thickness has little effect on the fitability of the formed sheet. Combined with the wall thickness distribution (STH) and equivalent plastic. strain diagram (PEEQ) of Figure 22, it can be found that the equivalent plastic strain value of the sheet in the punch contact area decreases gradually with the increase of the upper sheet thickness, the strain distribution and the wall thickness distribution of the corresponding parts are more uniform. The position where the sheet produces the maximum plastic strain is located in the part suspending area. The difference between the maximum and minimum equivalent plastic strain of the sheet represents the uniformity of sheet forming. The strain difference values under different thicknesses of upper sheets were 0.609, 0.503 and 0.599, respectively. Therefore, the forming wall thickness of the formed sheet under the condition of 1.5 mm upper sheet is more uniform.

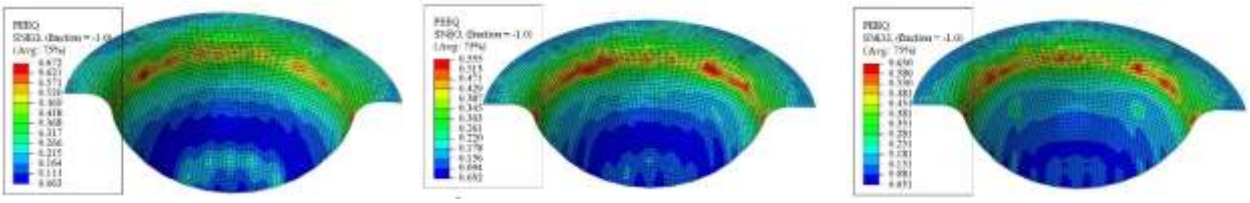

(a) 1 mm (b) 1.5 mm (c) 2 mm

Fig. 22 The wall thickness and equivalent plastic strain with different thickness of upper sheet

5.5 Influence of different temperatures on part formability

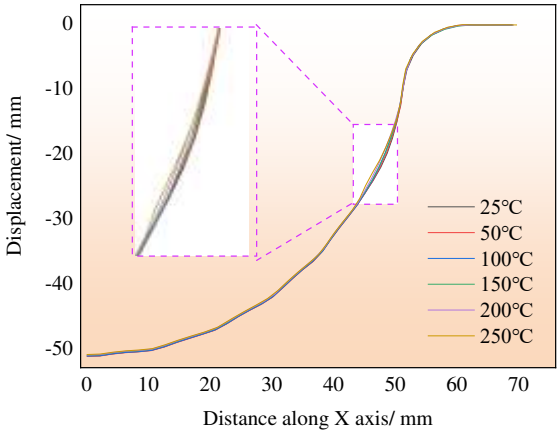

Fig. 23 Part Outline at Different Temperatures

In order to further optimize the forming quality of the suspending area of hemispherical parts, this section introduces warm forming technology to process the parts. Warm forming technology refers to heating the sheet and die to the target temperature for stamping [17]. This section set 25℃、50℃、100℃、150℃、200℃、250℃ six temperature for the simulation of double-layer sheet hydroforming.

It can be found from the contour diagrams of the parts at different temperatures in Figure 23 that the higher the temperature, the better the fitting property of the parts. Combined with Figure 24, it can be seen that the temperature can improve the thinning of the suspending area of the part. The wall thickness of the suspending area of the part was 0.4673 mm at 25 °C. With the increase of temperature, the wall thickness of the suspended area increases gradually, and the wall thickness of the suspending area reached 0.5030 mm at 250 °C. This is mainly due to the high temperature softening effect of the sheet at 250 °C, which greatly improves the flowability of the sheet. In the range of 50 ~ 200 °C, the minimum wall thickness of the sheet has little difference, but at 250 °C, the thinning of the ball bottom suddenly increased, which is due to the high temperature softening effect of the sheet, leads to the decrease of the strength of the sheet and makes the sheet thinning seriously in the inverse bulging stage. According to the wall thickness distribution and the minimum wall thickness value of the parts, the best forming temperature is 150 °C.

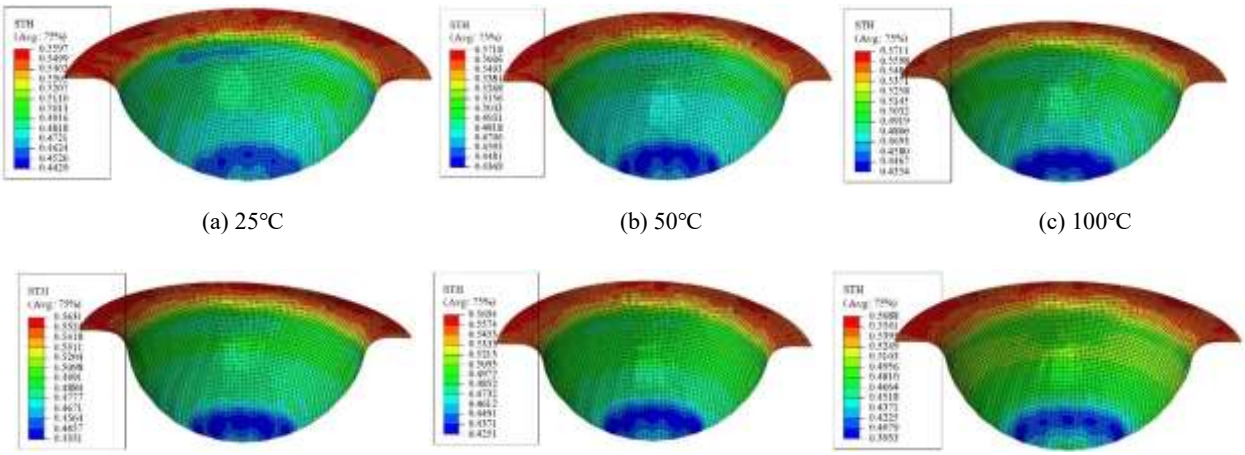

(a) 25℃ (b) 50℃ (c) 100℃

(d) 150℃ (e) 200℃ (f) 250℃

Fig. 24 Wall Thickness Distribution of Parts at Different Temperatures

6. Experimental study on double-layer sheet hydroforming

6.1 Experimental scheme design

In this paper, the experimental verification using

200t hydraulic deep drawing equipment, mainly composed of hydraulic system, forming system, control system, as shown in Figure 25 equipment. The device can display the instantaneous hydraulic pressure, punch displacement and other parameters in the forming process, which is conducive to the control and adjustment of various parameters.

This experiment uses 40Cr stainless steel mold, domestic 20 # hydraulic oil as chamber liquid. Before the experiment starts, the heating furnace can be used to heat the mold. The formed sheet is a 6061-T6 aluminum alloy rolling plate with a thickness of 0.5 mm. The upper sheet is 1Cr18Ni9Ti plate, and the diameter of the sheet is 170 mm. The upper sheet was stacked on the formed sheet for hydroforming, and the surface of the upper sheet was treated, so that the friction coefficient between the two sheet reached 0.1. The initial parameters were set as follows : blank holder gap was 2.2 mm, pre-bulging pressure was 4 MPa, and maximum hydraulic pressure was 20 MPa. Apply lubricating oil in the contact area of die and blank holder to ensure the fluidity of sheet at the beginning of forming.

Fig.25 Stamping equipment

The formed parts were cut along the diameter direction by wire cutting, and eight measuring points were taken on average from the center of the parts to the edge of the sheet as shown in Figure 26. The wall thickness of parts was measured by ultrasonic thickness gauge.

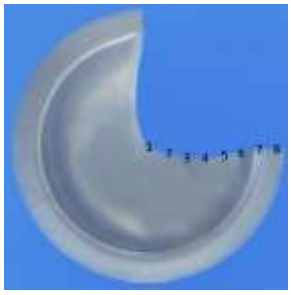

Fig. 26 Forming part

6.2 Effect of upper sheet on part wall thickness

In this section, the hydroforming experiments of the parts without upper sheet，1 mm upper sheet, 1.5 mm upper sheet and 2 mm upper sheet were carried out respectively. The forming diagram of the parts and the wall thickness value of the measuring point are shown in Figure 27.

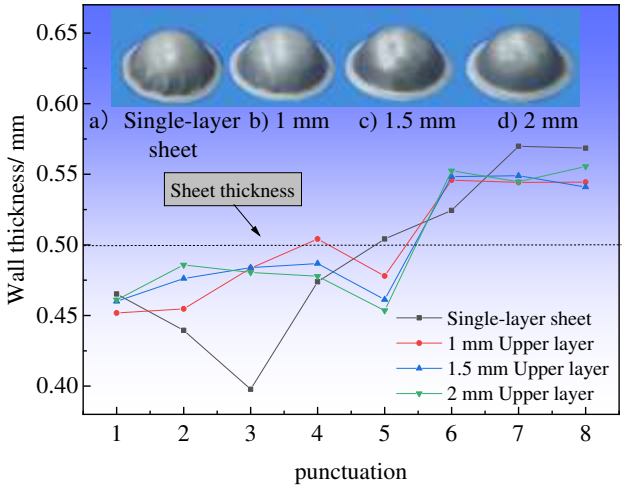

Fig. 27 Comparison of formed parts and wall thickness under different upper sheet

From Figure 27, it can be seen that the part bottom is thinned seriously when the single-layer sheet is formed by hydroforming. At the same time, with the defect of wrinkle in the suspending area. the wall thickness of the part bottom is obviously improved by double-layer sheet hydroforming. The maximum thinning rate of the part is far lower the single-layer sheet forming, and the wall thickness uniformity of the part is also improved. Observe the

forming conditions of parts with different upper sheet thickness. When the upper sheet was 1 mm, the wrinkling in the suspending area of the parts was not completely inhibited. When the upper sheets were 1.5 mm and 2 mm, the suspending area of the formed parts was smooth and flat, and the wrinkling in the suspending area of the hemispherical parts was effectively improved.

6.3 Effect of temperature on wall thickness of parts

In this section, the forming experiments were carried out at room temperature and 150 °C respectively. The thickness of the upper sheet was 1.5 mm, and the part diagram and wall thickness comparison diagram are shown in Figure 28. The part had good formability at room temperature and 150 °C. Due to the temperature, the plasticity of the sheet is enhanced. Under the hydraulic pressure, the degree of inverse bulging at the ball bottom in the pre-bulging stage increases, and the wall thickness thinning rate increases. At the same time, the flowability of sheet increases. Under the same process parameters, the trend of sheet flowing into the formed area from the unformed area increases. At 150 °C, the wall thickness thickening rate of the part flange area decreases, which was easier to make the sheet flow into the die and improve the wall thickness thinning of the part suspending area.

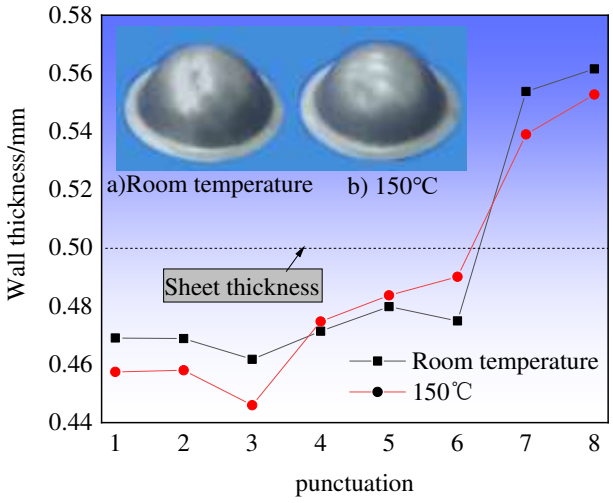

Fig. 28 Comparison of forming parts and wall thickness under different temperature

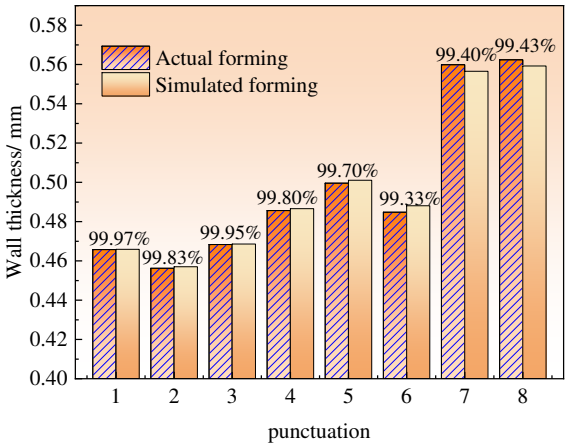

Fig. 29 The comparison of simulation results with actual results

6.4 Simulation accuracy verification

In order to explore the accuracy of numerical simulation, the forming wall thickness of the part under the condition of 1.5 mm upper sheet at room temperature was compared with the wall thickness obtained by simulation, as shown in Figure 29. It can be obtained from the figure that the wall thickness of the part obtained in actual production is consistent with the simulation results. The minimum wall thickness occurs at the part bottom, and the simulation accuracy reaches 99.33 %.

7. Conclusion

In this paper, the deformation characteristics of 6061 - T6 aluminum alloy were investigated by uniaxial tensile test, and the constitutive model of the material was constructed based on BP neural network. The constitutive model was imported into ABAQUS software to simulate the double-layer sheet hydroforming, and the optimal forming parameters were obtained. The accuracy of the simulation was verified by experiments. The conclusions are as follows:

1. Compared with the experimental data obtained by uniaxial tensile test and the data predicted by BP neural network model, the overall error is within 5 %, the minimum error is 0.05 %, and the average error is 0.92 %. The fitting coefficient of the two is 0.9982, which has a high correlation. Therefore, the constitutive model based on BP neural network can accurately characterize the deformation characteristics

of 6061 - T6 aluminum alloy. The introduction of this constitutive model can effectively improve the simulation accuracy of the simulation software.

2. Increasing the hydraulic pressure can improve the moldability of the hemispherical parts and improve the wrinkle problem of the suspended area of the parts, but it will cause the problem of wall thickness thinning and even rupture. By analyzing the wall thickness distribution and fittability of the parts, the optimum maximum hydraulic pressure was 20 MPa and the optimum pre-bulging pressure was 4 MPa.

3. By comparing the parts formed by hydraulic deep drawing of single-layer sheet and double-layer sheets, the existence of upper sheet makes the plastic strain of the whole plate more uniform, improves the wall thickness uniformity of the parts, and reduces the maximum thinning rate of the parts.

4. Selected 1Cr18Ni9Ti stainless steel as the upper sheet, the appropriate thickness of the upper sheet can control the fracture and wrinkle of the suspending area. The appropriate friction coefficient between the sheets can reduce the blocking effect of the die and blank holder on the flow of the sheet to the forming area, and obtain the parts with better quality. By comprehensive comparison, the best outer coating thickness is 1.5 mm, and the best friction coefficient is 0.1.

5. Temperature increases the plasticity of the sheet, decreases the yield strength, and increases the degree of inverse bulging thinning in the pre-bulging stage. The flowability of sheet metal from unformed area to formed area increases, and the uniformity of parts in suspended area and flange area increases.

6. The test of upper sheets with different thicknesses was carried out by using the optimal process parameters. The results showed that the existence of upper sheets could significantly improve the wrinkle problem in the suspending area of the parts, temperature can improve the wall thickness uniformity of the plate in the suspended area. At the same time, the experimental results are basically consistent with the wall thickness values obtained by data and numerical simulation, and the simulation accuracy reaches 99.33 %.

Ethics declarations

Ethical Approval

Not applicable

Consent to Participate

Not applicable

Consent to Publish

Not applicable

Authors Coutributions

Zhi He Zhang: Conceptualization, Methodology, Writing- Original draft preparation, Experimental scheme design. Xiao Jing Liu: Writing- Reviewing and Editing. Xue Feng Ma: Experiment. Chao Li: Verification. Validation. Ying Ying Zhou: Supervision.

Funding information

This paper was financially Supported by Harbin academic leader fund (2017RAXXJ008) and National natural science foundation of China (51975167).

Competing Interests

Not applicable

Availability of data and materials

The data obtained in the framework of this study are available to the journal upon request.

Reference

1 Mahabunphachai S, Koç M (2010) Investigations on forming of aluminum 5052 and 6061 sheet alloys at warm temperatures. Mater Des 31(5): 2422–2434. DOI: 10.1016/j.matdes.2009.11.053

2 F. Ozturk, A. Sisman, S. Toros, S. Kilic, R.C. Picu (2010) Influence of aging treatment on mechanical properties of 6061 aluminum alloy.

Mater Des 31(2):972–975. DOI: 10.1016/j.matdes.2009.08.017

3 V. SENTHILKUMAR, A. BALAJI, D. ARULKIRUBAKARAN (2013) Application of constitutive and neural network models for prediction of high temperature flow behavior of Al/Mg based nanocomposite. Trans. Nonferrous Met. Soc. China 23(6):1737–1750. DOI: 10.1016/S1003-6326(13)62656-4

4 Qin Xiang Xia, Shi Xian Chen, Xin Zhu (1992) Composite Laminates and Their Applications. Forging and Stamping Technology. DOI:10.13330/j.issn.1000-3940.1992.06.005

5 Bin Jun Zhou, Yong Chao Xu, Zhi Chao Zhang, Lan Hu(2020) Research Development for Deep Drawing of Multilayer Sheet Metals. Mater Rep 34(23): 23165-23170. DOI: 10. 11896 / cldb. 19100085

6 Hao Dong (2015) Investigation on hydro-forming of 5A06 aluminum alloy double-layer sheets. Harbin Institute of Technology 2015: 1-77.

7 Jiu Hong Zhou (2016) Research on hydroforming of double layered sheet of inner tailor-welder blank of 2219 aluminum alloy. Harbin Institute of Technology 2016: 1-49.

8 Zhi Chao Zhang, Yong Chao Xu, Shi Jian Yuan (2016) Effect of outer stainless steel on the deformation behavior of hydro-bulging of 5A06 aluminum alloy sheet. Journal of Mechanical Engineering 52(14): 40-47. DOI：10.3901/JME.2016.14.040

9 Yong Chao Xu, Bin Jun Zhou, Jiu Hong Zhou (2016) Effects of outside sheet on the bulging properties of inside 2219 aluminum FSW Sheet. Journal of Netshape Forming Engineering 2016, 8(05): 65-70. DOI：10.3969/j.issn.1674-6457.2016.05.010

10 Tie Jun Gao, Yang Liu, Peng Chen, Zhong Jin Wang (2015) Analysis of bulging process of aluminum alloy by overlapping sheet metal and its form ability. Transactions of Nonferrous Metals Society of China 25(4): 1050-1055. DOI: 10.1016/S1003-6326(15)63697-4

11 Bin Jun Zhou, Yong Chao Xu (2016) Wrinkle behavior of hydroforming of aluminum alloy double-layer sheets. The Journal of the Minerals, Metals & Materials Society 68(12): 3201–3207. DOI: 10.1007/s11837-016-2025-8

12 Bin Jun Zhou, Yong Chao Xu (2018) The effect of upper sheet on wrinkling and thickness distribution of formed sheet part using double-layer sheet hydroforming. The International Journal of Advanced Manufacturing Technology 99(5-8): 1175-1183. DOI: 10.1007/s00170-018-2432-9

13 Bin Jun Zhou, Yong Chao Xu, Zhi Chao Zhang (2020) Research on the selection principle of upper sheet in double-layer sheet hydroforming. The International Journal of Advanced Manufacturing Technology 109(7): 1663-1669. DOI: 10.1007/s00170-020-05615-0

14 Alireza JALIL, Mohammad HOSEINPOUR GOLLO, M. Morad SHEIKHI, S.M. Hossein SEYEDKASHI (2016) Hydrodynamic deep drawing of double layered conical cups. Transactions of Nonferrous Metals Society of China 26(1):237–247. DOI: 10.1016/S1003-6326(16)64109-2

15 M. Molaei, M. Safaria, H. Deilami Azodi, J. Shahbazi Karami (2018) Experimental and Numerical Investigations of Hydromechanical Deep Drawing of a Bilayer Conical Cup. Journal of Stress Analysis 3(1):53-60. DOI: 10.22084/jrstan.2018.16084.1046

16 Xiao Jing Liu, Yong Chao Xu (2007) Numerical simulation of hydrodynamic deep drawing with independent radial hydraulic pressure of aluminum alloy cylindrical cup with a hemispherical bottom. Journal of Harbin institute of technology 09:1402-1406.

17 Koc Muammer, Agcayazi Ali, Carsley John (2011) An Experimental Study on Robustness and Process Capability of the Warm Hydroforming Process. J Manuf Sci Eng 133(2): 021008. DOI: 10.1115/1.4003619